

Retraction dynamics of aqueous drops upon impact on nonwetting surfaces.

By DENIS BARTOLO¹ CHRISTOPHE JOSSERAND² and DANIEL BONN^{1,3}

¹Laboratoire de Physique Statistique de l'ENS, 24 Rue Lhomond, 75231 Paris cedex 05, France

²Laboratoire de Modélisation en Mécanique, CNRS-UMR 7606, Case 162, 4 place Jussieu, 75252 Paris Cédex 05-France

³ van der Waals-Zeeman Institute, University of Amsterdam, Valckenierstraat 65, 1018 XE Amsterdam, The Netherlands

(Received 20 August 2018)

We study the impact and subsequent retraction dynamics of liquid droplets upon high-speed impact on hydrophobic surfaces. Performing extensive experiments, we show that the drop retraction rate is a material constant and does not depend on the impact velocity. We show that when increasing the Ohnesorge number, $Oh = \eta/\sqrt{\rho R_i \gamma}$, the retraction, *i.e.* dewetting, dynamics crosses over from a capillaro-inertial regime to a capillaro-viscous regime. We rationalize the experimental observations by a simple but robust semi-quantitative model for the solid-liquid contact line dynamics inspired by the standard theories for thin film dewetting.

1. Introduction: Drop Impact on Solid Surfaces

Drops impacting onto solid surfaces are important for a large number of applications: for instance, almost all spray coating and deposition processes rely ultimately on the interaction of a droplet with a surface. A large variety of phenomena can be present during drop impacts, from splashes to spreading, and from large wave surface deformation to rebound (see (Rein 1993) and references therein).

Research on drop impacts has a long history, starting with the pioneering studies of Worthington and later on with the famous photographs of Edgerton (Worthington 1876; Edgerton & Killian 1954). Most of the previous work on drop impact focused on determining the maximum diameter a drop is capable of covering upon impact (Fukai *et al.* 1993; Roisman *et al.* 2002; Clanet *et al.* 2004). However, the practical problem of deposition can be very different if one wants to efficiently deposit some material on the surface. This is especially grave when the surface is not wetted by the liquid, as is illustrated by the high-speed video pictures in Fig.1 for the impact of a water droplet. It can be observed that the drop expands rapidly, due to the large speed with which it arrives at the surface. However, due to the hydrophobicity of the surface, subsequently the drop retracts violently, leading to the ejection of part of the droplet from the surface: we observe droplet rebound. It is this "rebound" that is the limiting factor for deposition in many applications, for instance for the deposition of pesticide solutions on hydrophobic plant leaves (Bergeron *et al.* 2000). We study here the impact and subsequent retraction of aqueous drops onto a hydrophobic surface, and seek to understand the dynamics of expansion and retraction of the droplets.

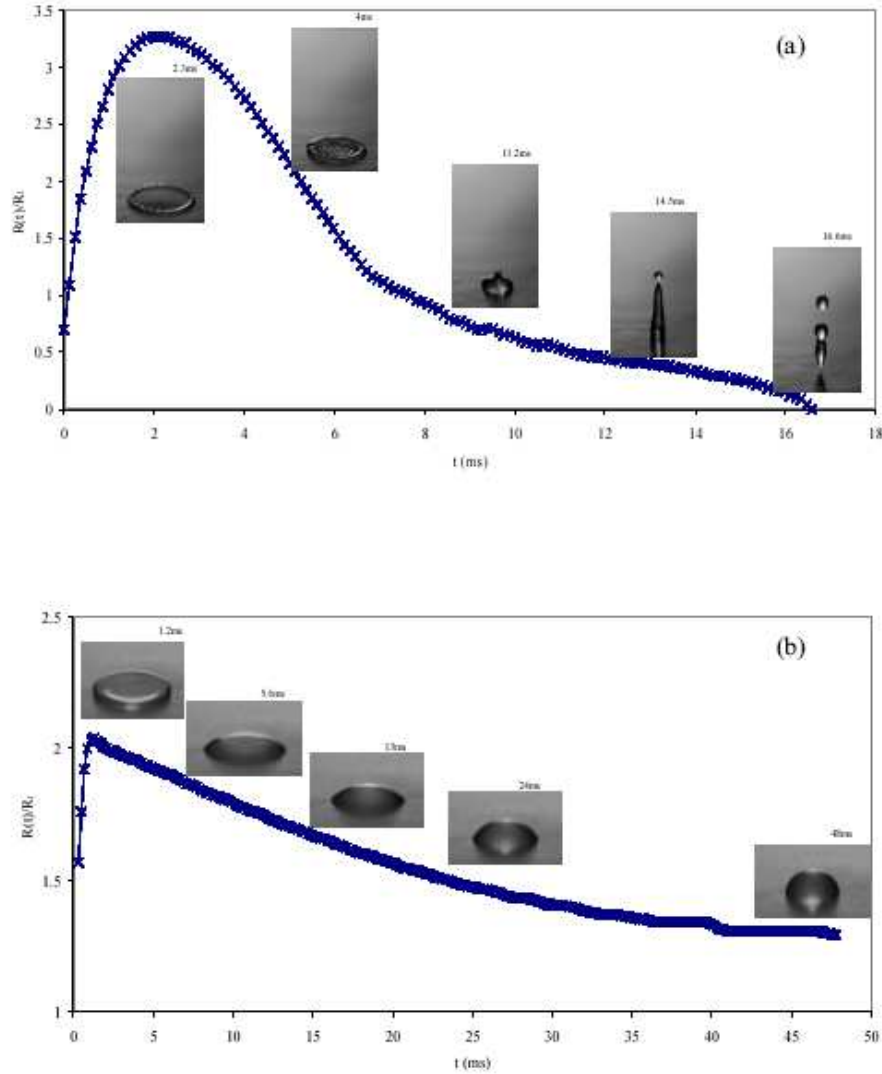


FIGURE 1. Temporal evolution of the contact radius of droplets upon impact and retraction. The radii are normalized by those of the spherical droplets before impact. The pictures show the shape of the droplets at the different stages of retraction. Droplet radius is 1 mm , impact speed is $2 \text{ m} \cdot \text{s}^{-1}$: a) pure water, b) viscous water-glycerol mixture, viscosity $50 \text{ mPa} \cdot \text{s}$.

In general, these problems are difficult because for most practical and laboratory situations, three forces play an important role: the capillarity and viscous forces, and the inertia of the droplets. We try and disentangle the effects of the three forces here by performing systematic experiments, varying both the importance of viscous and inertial forces.

We provide experimental evidence for the existence of two distinct retraction regimes. In both regimes, capillary forces are the motor behind the droplet retraction, and are, for the first regime countered by inertial forces. In the second regime the main force slowing down the retraction is viscous. We also show that, perhaps surprisingly, the drop

retraction rate (the retraction speed divided by the maximum radius) does not depend on the impact velocity for strong enough impacts. The dimensionless number that governs the retraction rate is found to be the Ohnesorge number, $Oh = \eta/\sqrt{\rho R_I \gamma}$, with η the viscosity, ρ the liquid density, R_I the impacting drop radius, and γ the surface tension. The Ohnesorge number therefore compares the dissipative (viscous) forces to the non-dissipative (capillary and inertial) forces. The crossover between the two regimes is found to happen at a critical Ohnesorge number on the order of 0.05 .

In order to develop a better understanding for the different regimes that are encountered, particularly the retraction dynamics in these regimes, we propose two simple hydrodynamic models inspired by the standard description of thin film dewetting dynamics. These simple models provide a simple but quite robust picture that allows us to rationalize the retraction rate in both regimes.

In order to be able to say something about the speed of retraction, one also needs to understand the maximum radius to which the droplet expands. Combining our results with those obtained by (Clanet *et al.* 2004) for the maximum radius, we propose a phase diagram delimiting four regions for the spreading and retraction dynamics of impacting drops.

2. Drop retraction dynamics: Generic Features

As the impact dynamics of liquid droplets on a solid surface happens usually in a few tens of milliseconds, we use a high-speed video system (1000 frames/second, Photonetics) to analyze the drop-impact events. When necessary, we use an ultrahigh-speed system allowing to go up to 120,000 frames/second (Phantom V7). We study aqueous drops impacting on a solid surface; the surface we used is Parafilm, which provides us with a hydrophobic surface (receding contact angle for water $\theta_R \approx 80^\circ$). In addition, the surface has a low contact angle hysteresis with water, and allows us to obtain highly reproducible results. The liquids we used are different water-glycerol mixtures. Varying the glycerol concentration, we vary the liquid viscosity, keeping the liquid density and its surface tension almost constant. For the highest concentration of glycerol, the surface tension has decreased from 72 (pure water) to 59 mNm^{-1} , whereas the density has increased to 1150 kg/m^3 . The viscosity is varied between 1 and 205 mPas. Viscosity, density and surface tension were measured before each impact experiment. Drops were produced using precision needles, and the initial radius of the drops R_I have been systematically measured on the images ($1.1 < R_I < 1.4$ mm). From the high-speed images such as the ones shown in Fig.1, we follow the contact radius R in time. This section summarizes the results of more than 80 different drop impact experiments, each of which have been repeated at least two times.

Two series of experiments were performed: first, letting the droplets fall from a fixed height, but increasing the viscosity, we increase the Ohnesorge number while keeping the inertial forces constant. The second series of experiments is performed at fixed viscosity and upon increasing the height from which the droplets falls; the droplet turns out to be in free fall (as is verified in the experiment to within a few percent) and so the relation between fall height h and impact velocity is simply $V_I = \sqrt{gh}$, with g the gravitational acceleration. Increasing the impact velocity increases the Weber number, keeping the Ohnesorge number fixed, where the Weber number, We , compares the inertial forces to the capillary forces, $We \equiv \rho R_I V_I^2 / \gamma$.

In all that follows, we restrain ourselves to high-speed impact conditions. More precisely, the Weber and Reynolds numbers are chosen so that $We > 10$ and $Re > 10$, where $Re \equiv \rho R_I V_I / \eta$ is the Reynolds number. This implies that inertial forces are at least one

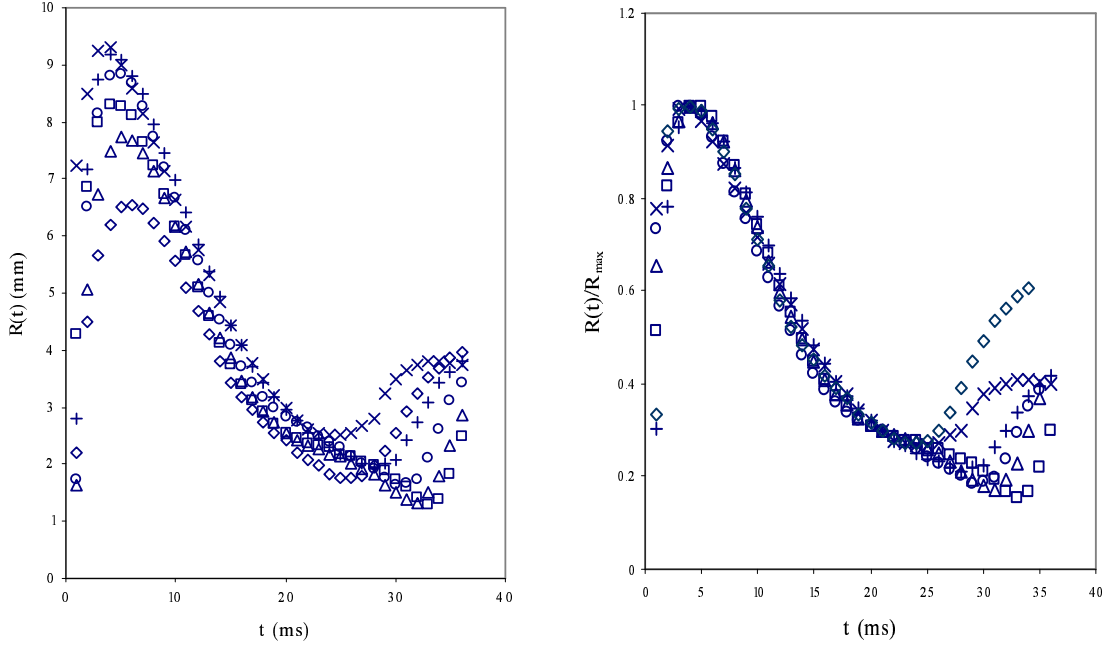


FIGURE 2. Temporal evolution of the contact radius for a water-glycerol drop $Oh = 9.1 \cdot 10^{-2}$, $R_I = 1.2$ mm (a) contact radius vs. time, (b) contact radius normalized by the maximum spreading radius vs. time Impact velocities : \times : $V_I = 2.4 \text{ms}^{-1}$, $+$: $V_I = 2.2 \text{ms}^{-1}$, \circ : $V_I = 1.9 \text{ms}^{-1}$, \square : $V_I = 1.7 \text{ms}^{-1}$, Δ : $V_I = 1.4 \text{ms}^{-1}$, \diamond : $V_I = 1 \text{ms}^{-1}$

order of magnitude larger than both the capillary and the viscous forces. Such conditions imply large deformations of the drop when the liquid impinges on the solid substrate. On the other hand, we also restrain our experiments to impact speeds that are far from the ‘splashing’ regime in which the drop disintegrates after impact to form a collection of much smaller droplets (Mundo *et al.* 1995).

The pictures in Fig.1 show that two distinctly different regimes exist for the shape of the droplets after impact. For low fluid viscosity, we typically obtain the images shown in Fig.1(a). At the onset of retraction, almost all of the fluid is contained in a donut-shaped rim, with only a thin film of liquid in the center. On the other hand, for high viscosities the deformation of the drop is less important, and the pancake-shaped droplet of Fig.1(b) results. These visual observations allow to distinguish the capillary-inertial and the capillary-viscous regimes that are described in detail below directly.

2.1. Drop Retraction Rate: influence of fall height and viscosity

Fig. 2 summarizes the most important findings of this study. The temporal evolution of the drop contact radius $R(t)$ for different impact velocities, shown in (a), is normalized in (b) by its maximal value at the end of the spreading R_{\max} . Two important observations are made. (i) A well defined retraction velocity V_{ret} can be extracted from each experiment; this is a non-trivial observation that will be rationalized below. (ii) Independently of the impact speed, all the $R(t)/R_{\max}$ curves collapse onto a single curve for different impact velocities. This shows that the retraction *rate*, rather than the retraction speed is the natural quantity to consider, and that this rate is independent of the impact velocity. These results hold for all the viscosities tested in our experiments.

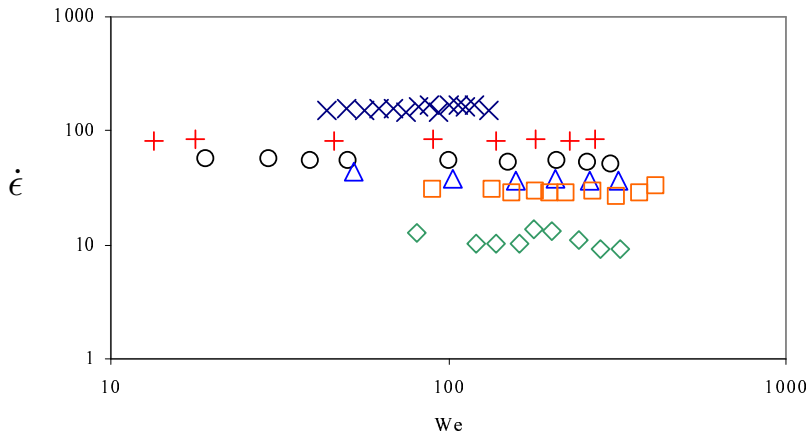


FIGURE 3. Retraction Rate plotted versus Impact Weber number for various water glycerol droplets. \times : $Oh = 2.510^{-3}$, $+$: $Oh = 3.910^{-3}$, \circ : $Oh = 1.510^{-2}$, \triangle : $Oh = 1.610^{-2}$, \square : $Oh = 2.310^{-2}$, \diamond : $Oh = 7.110^{-2}$

In Fig. 3 we have plotted the retraction rate $\dot{\epsilon} \equiv V_{\text{ret}}/R_{\text{max}}$ versus the impact Weber number, where V_{ret} is defined by $V_{\text{ret}} \equiv \max[-\dot{R}(t)]$. Clearly, the drop retraction rate does not depend on the impact velocity. One might think that the explanation for this observation is rather obvious: the initial kinetic energy of the droplet is transformed into surface energy (which fixes $R_{\text{max}}/R_I \propto We^{1/2}$), and is then transformed back into kinetic energy (which in turn fixes $V_{\text{ret}} \propto V_I$). This naive explanation is unfortunately wrong from the following reasons. First, it has been observed recently that, at the onset of retraction, low viscosity liquids undergo vortical motion in the drop (Clanet *et al.* 2004). This residual flow in the drop reveals that a part of the initial kinetic energy is still available then, and thus that a simple energy balance argument cannot work. This was indeed already suggested by previous observations of a clear disagreement between experiments and the $R_{\text{max}}/R_I \propto We^{1/2}$ law (Fukai *et al.* 1993; Roisman *et al.* 2002; Okumura *et al.* 2003). The second reason why the simple energy-balance argument does not work follows directly from Fig. 3, where it is shown that the retraction rate depends on the viscosity and consequently that the previous inviscid picture is not correct.

We therefore performed experiments that elucidate the role of the viscosity, or, equivalently, of the Ohnesorge number. For what follows, it is convenient to define two intrinsic time scales for the droplet: a viscous one and an inertial one. The viscous time is the relaxation time of a large-scale deformation of a viscous drop: $\tau_v \equiv (\eta R_I)/\gamma$, whereas the inertial time scale: $\tau_i = (\frac{4}{3}\pi\rho R_I^3/\gamma)^{1/2}$ corresponds to the capillary oscillation period of a perturbed inviscid droplet. Since τ_i is independent of V_I and η , this quantity is almost constant for all tested drops.

Fig. 4 shows the retraction rate, made dimensionless using the inertial time, as a function of the Ohnesorge number. It can be observed in the figure that two different regimes exist for the retraction rate. The first region where the retraction rate $\dot{\epsilon}$ is independent of the viscosity points to an inertial regime and $\dot{\epsilon} \propto \tau_i^{-1}$. The retraction rate is consequently found not to depend on the impact speed, a result similar to that obtained recently by (Richard *et al.* 2002) who show that the contact time is independent of the impact speed. For higher viscosities, typically $Oh > 0.05$, the retraction rate decreases strongly. In this regime, capillary and viscous forces govern the dynamics: we find $\dot{\epsilon} \propto \tau_v^{-1}$.

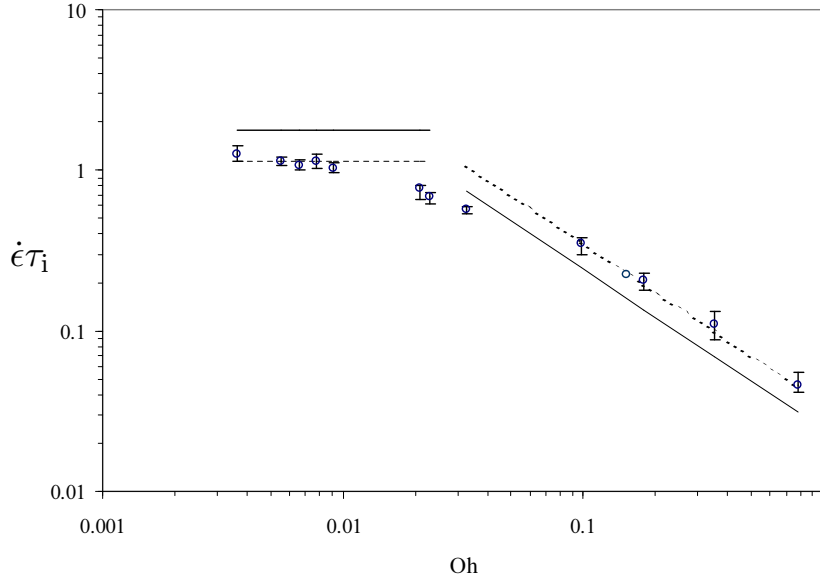


FIGURE 4. Circles: Normalized retraction rate $\dot{\epsilon}\tau_1$ plotted versus the Ohnesorge number, experimental values. Error bars represent the maximum deviation from the mean value. Full line: (left) $\dot{\epsilon}\tau_1$ evaluated using Eq. 3.2, (right) $\dot{\epsilon}\tau_1$ evaluated using Eq. 3.6. Dashed line : (left) Fit obtained taking the mean value of the five first experimental points, (right) Best fit according to the predicted $1/Oh$ power law.

3. Two simple models for the drop retraction dynamics

We have consequently established the existence of two different regimes for the retraction rate: a viscous one and an inertial one. We now develop some simple arguments allowing for a semi-quantitative description of the dynamics, using ideas already existing for the dynamics of dewetting, a problem closely related to the current one.

3.1. Inertial regime

We employ a Taylor-Culick approach commonly used for the inertial dewetting of thin films (Taylor 1959; Culick 1960; Buguin *et al.* 1999) to describe the drop retraction rate. For high-velocity drop impacts, liquid spreads out into a thin film of thickness h and radius R_{\max} . The liquid subsequently dewets rapidly the surface, and in doing so forms a rim that collects the liquid that is initially stored in the film. The shape of the drop surface shape is therefore never in a steady state and consists of a liquid film formed during the spreading stage and a receding rim. The contact angle at the outer side of the rim is taken to be very close to the receding contact angle (θ_R) since viscous effects can be neglected small (Buguin *et al.* 1999). The dynamics is consequently determined by a competition between capillary tension coming from the thin film and the inertia of the rim. If we write down momentum conservation for the liquid rim:

$$\frac{d}{dt} \left(m \frac{dR(t)}{dt} \right) = F_C \quad (3.1)$$

with m the mass of the liquid rim and F_C the capillary force acting on it, $F_C \sim 2\pi\gamma R(t) [1 - \cos(\theta_R)]$. The stationary solution of Eq.3.1 can be obtained writing $\dot{m}(t) =$

$2\pi\rho R V_{\text{ret}} h$, and gives: $V_{\text{ret}} = \sqrt{\gamma[1 - \cos(\theta_R)]/(\rho h)}$. Using volume conservation, $h \sim \frac{4}{3}R_I^3 R_{\text{max}}^{-2}$, it follows that:

$$\frac{V_{\text{ret}}}{R_{\text{max}}} \sim \tau_i^{-1} \sqrt{\pi [1 - \cos \theta_R]} \quad (3.2)$$

Which is the final result. Comparing with the experimental data, it turns out that this equation not only gives the correct scaling behavior for the retraction in this regime rate but also provides a rather accurate estimate of the numerical prefactor (see Fig 4). Indeed, the ratio between the experimental and the predicted numerical prefactors is found to be 0.6 Repeating the experiment for water on a polycarbonate surface, which changes the contact angle value to 60° , we retrieve exactly the same ratio of 0.6.

3.2. Viscous regime

In the opposite limit of very viscous liquids, the drops adopt pancake shapes upon impact. During the first stages of retraction, the pancake shape rapidly relaxes towards a roughly spherical cap, and the drop shape remains like this during the retraction since the capillary number is small. During the retraction, it is only the contact angle that varies slowly: it is mainly this slow contact angle dynamics that dictates the drop evolution during the retraction. Contrary to the previous analysis, the slow receding velocity allows to assume a quasi-static dynamics for the surface shape during the retraction. In this regime, it is then natural to assume that the work done by the capillary force F_C is dissipated through viscous flow near the contact line. Since we focus our study on high-speed impacts, R_{max} is always much larger than R_I which justifies a small $\theta(t)$ approximation at the onset of retraction. The viscous effects near the contact line then lead to the well-known linear force-velocity relation (DeGennes 1985):

$$F_V = -\frac{6\pi\eta}{\theta} \ln\left(\frac{\Lambda}{\lambda}\right) R(t)\dot{R}(t) \quad (3.3)$$

where Λ and λ are respectively a macroscopic and a microscopic cutoff lengths. Λ is typically of the same order as the drop size $\sim 1\text{mm}$. λ is a microscopic length, and is usually taken to be on the order of $\lambda \sim 1\text{nm}$ (DeGennes 1985). On the other hand, the capillary force drives the retraction. Near the contact line it can be written:

$$F_C = 2\pi R(t)\gamma [\cos \theta(t) - \cos \theta_R] \quad (3.4)$$

Volume conservation gives: $\frac{4}{3}\pi R_I^3 \sim \frac{\pi}{4}\theta(t)R^3(t)$, where we have taken the small angle limit. Eqs. 3.3 and 3.4 together with the volume constraint leads to the following relation for the variation of the contact radius:

$$\frac{\dot{R}(t)}{R(t)} = -\frac{[1 - \frac{1}{2}\theta^2(t) - \cos(\theta_R)] \theta(t)^{4/3}}{(144)^{1/3} \ln(\Lambda/\lambda)} \tau_v^{-1} \quad (3.5)$$

the above equation is obtained in the small angle limit and is only valid for short time after the onset of retraction. We estimate the retraction rate $\dot{\epsilon}$ as the maximum value of $\dot{R}(t)/R(t)$ so that:

$$\frac{V_{\text{ret}}}{R_{\text{max}}} \approx \left(\frac{3}{25}\right)^{1/3} \frac{(1 - \cos \theta_R)^{5/3}}{5 \ln(\Lambda/\lambda)} \tau_v^{-1} \quad (3.6)$$

Comparing again to the experiments, good agreement is found: the retraction rate is solely set by the viscous relaxation time τ_v and consequently $\dot{\epsilon}\tau_i \propto Oh^{-1}$. Beyond this correct scaling prediction, Eq. 3.6 provides a quite accurate estimate for the numerical prefactor as is shown in Fig 4. Indeed, the ratio between the experimental and the

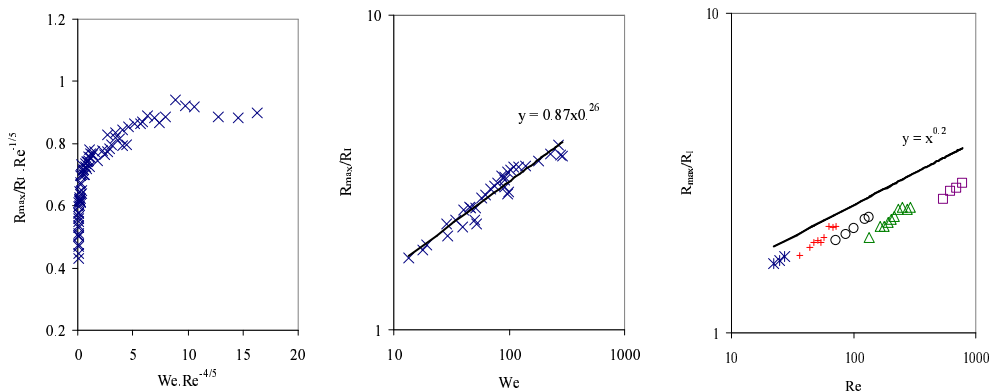


FIGURE 5. (a) Normalized maximum spreading radius plotted vs. the impact number. (b) R_{\max} (normalized by the radius before impact) plotted vs. Weber number for small values of the impact number. Full line: power-law fit. (c) R_{\max} (normalized by the radius before impact) plotted vs. Reynolds number for large values of the impact number. Full line: predicted power-law dependence with power 0.2. *: $\eta = 10^{-1} Pa.s$, +: 9.510^{-2} , o: $4.810^{-2} Pa.s$, Δ : $\eta = 2.810^{-2} Pa.s$, \square : $\eta = 10^{-2} Pa.s$

predicted numerical prefactors is found to be 1.5. Again, repeating the experiment on a polycarbonate surface, this ratio changes only slightly from 1.5 to 1.8.

4. Conclusions and perspectives

Our experiments reveal that the retraction rate is independent of the impact speed. To account for the retraction speed, the maximum radius to which the droplet expands, has to be known also. A number of studies have been devoted to the understanding of the maximum spreading radius (see for instance (Fukai *et al.* 1993; Roisman *et al.* 2002; Clanet *et al.* 2004)). However, no clear and unified picture emerges from previous experimental investigations. A recent experimental study of R_{\max} , combined with recent theoretical ideas in the same spirit of the ones presented here was done by Clanet *et al.* (2004). They obtain a zeroth order (asymptotic) description of the spreading stage, compare it with experiments and suggest that two asymptotic regimes exist for R_{\max} . The first is given by a subtle competition between the inertia of the droplet and the capillary forces; if only these two are important, it follows that $R_{\max}/R_I \propto We^{1/4}$. In the second regime, R_{\max} is given by a balance between inertia and viscous dissipation in the expanding droplet, leading to $R_{\max}/R_I \propto Re^{1/5}$. Consequently, a single dimensionless number is defined that discriminates between the two regimes: $P = WeRe^{-4/5}$ referred to as the Impact number. The crossover between the two regimes happens at a P of order unity.

Our experimental data are in qualitative agreement with their prediction, as is shown in Fig. 5.a. At low P , the scaling $R_{\max}/R_I \sim We^{1/4}$ is clearly observed. However, for impacts corresponding to $P > 1$, we observe only a very slow variation of the maximum spreading radius as a function of P . Therefore, the relation between R_{\max} and the Reynolds number is not very clear from our data (Fig 5. c). Although the main trend is not in strong contradiction with the prediction $R_{\max}/R_I \propto Re^{1/5}$, a power-law fit of our data gives exponents that are always smaller than the predicted value of 0.2. Perhaps even more important- in view of the small range of the maximal expansion R_{\max} that we cover- is that the different water-glycerol mixtures do not appear to collapse on a single master

curve, as would be predicted by the above argument. However, since the maximum value of P that we reach is on the order of 10, it may be that we have not reached the purely viscous regime. In that case, the capillary, inertial and viscous forces are still of comparable amplitude and have to be taken into account together. Note also that the more sophisticated models reviewed in Ukiwe & Kwok (2004) do not provide better agreement with our experimental measurements.

Despite this small problem, we are now able to develop a simple unified picture for drop impact dynamics accounting for both the spreading and the retraction dynamics. The two natural dimensionless numbers that have been identified are the impact number P , that quantifies the spreading out of the droplet, and the Ohnesorge number Oh that quantifies the retraction. We can thus construct a phase diagram in the experimentally explored (Oh, We) plane, which is shown on Fig. 6. The experimentally accessible plane is divided in four parts, where the main mechanisms at work during the impact process are different. These four parts are separated by the curves $Oh = 0.05$ and $We = Oh^{-4/3}$. They are labeled as follows: ICCI the drop dynamics is given by a competition between inertia and capillarity both for the spreading and the retraction. IVCV: inertia and viscous forces dominate the spreading, capillary and viscous forces dominate the retraction. These two regimes have been studied in detail here. The two more intriguing regions are the IVCI (viscous spreading, inertial retraction) and ICCV (capillary spreading, viscous retraction) that are unfortunately difficult to explore in detail. For the IVCI- regime, the large inertia at impact, combined with a small surface tension, will make the droplets undergo large non-axisymmetric deformations and they will eventually splash and disintegrate. On the other end of the phase diagram, the ICCV region corresponds to very low impact speeds and important capillary forces, implying very small deformations of the droplets. If the deformations are small, pinning of the contact line of the droplets will become important, and all our simple scaling arguments for both the maximum radius and the retraction rate are invalidated.

A numerical investigation of droplet impact would be very helpful for two reasons. First, numerics would allow to vary R_I while keeping all the other physical parameters constant. This would allow to check the robustness of our results, since experimentally it is not easy to vary R_I over a wide range. Second, as emphasized above, the viscous regime for the maximum radius is difficult to characterize precisely due to the smallness of the variation of R_{\max} for viscous drops. If precise numerical simulations could be done, these different remaining problems could be resolved.

In sum, we have studied the retraction dynamics of liquid droplets upon high-speed impact on non-wetting solid surfaces. Perhaps the strongest conclusion from our investigation is that the rate of retraction of the droplet is a drop constant which does not depend on the impact velocity. Two regimes for the retraction rate have been identified: a viscous regime and an inertial regime. We have in addition shown here that simple hydrodynamic arguments can be formulated that give very reasonable agreement with experiments in the two different regimes. **Acknowledgments:** Benjamin Helmann-Moussa is acknowledged for help with the experiments. Denis Bartolo is indebted to the CNRS for providing a post-doctoral fellowship. LPS de l'ENS is UMR 8550 of the CNRS, associated with the universities Paris 6 and Paris 7.

REFERENCES

- BERGERON, V., BONN, D., MARTIN, J.-Y. & VOVELLE, L. 2000 Controlling droplet deposition with polymer additives. *Nature* **405**, 772–775.

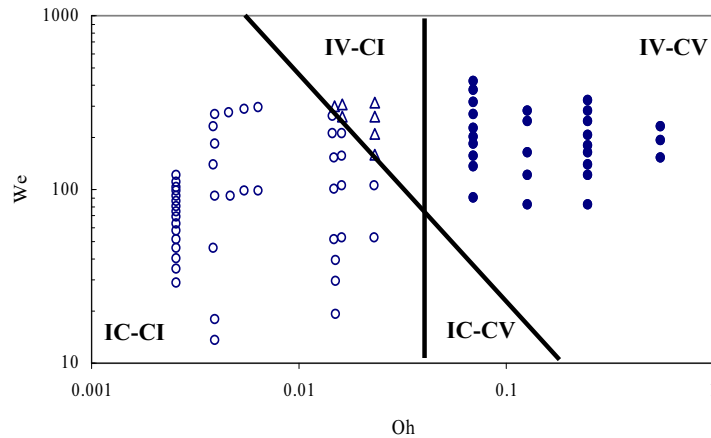


FIGURE 6. Phase diagram in the (We, Oh) plane for the impact and retraction dynamics of droplets. The four regions are discussed in the text, and the symbols represent the parameters of the data reported in this paper. Different symbols have been assigned for each region.

- BUGUIN, A., VOVELLE, L. & BROCHARD, F. 1999 Shock in inertial dewetting. *Phys. Rev. Lett* **83**, 1183–1186.
- CLANET, C., BÉGUIN, C., RICHARD, D. & QUÉRÉ, D. 2004 Maximal deformation of an impacting drop. *J. Fluid Mech.* **517**, 199–208.
- CULICK, F. E. C. 1960 Comments on a ruptured soap film. *J. Appl. Phys.* **31**, 1128.
- DEGENNES, P. G. 1985 Wetting: statics and dynamics. *Rev. Mod. Phys.* **57**, 827.
- EDGERTON, H. & KILLIAN, J. 1954 *Flash*. Charles T. Brandford Company, Boston.
- FUKAI, J., ZHAO, Z., POULIKAKOS, D., MEGARIDIS, C. M. & MIYATAKE, O. 1993 Modeling of the deformation of a liquid droplet impinging upon a flat surface. *Phys. Fluids* **5**, 2588–2599.
- MUNDO, C., SOMMERFELD, M. & TROPEA, C. 1995 Droplet-wall collisions: Experimental studies of the deformation and breakup process. *Int. J. Multiphase Flow* **21**, 151.
- OKUMURA, K., CHEVY, F., RICHARD, D., QUÉRÉ, D. & CLANET, C. 2003 Water spring: A model for bouncing drop. *Europhys. Lett.* **62**, 237–243.
- REIN, M. 1993 Phenomena of liquid drop impact on solid and liquid surfaces. *Fluid Dyn. Res.* **12**, 61.
- RICHARD, D., CLANET, C. & QUERE, D. 2002 Contact time of a bouncing drop. *Nature* **417**, 811–811.
- ROISMAN, I., RIBOO, R. & TROPEA, C. 2002 Normal impact of a liquid drop on a dry surface: model for spreading and receding. *Proc. R. Soc. Lond.* **458**, 1411–1430.
- TAYLOR, G. I. 1959 The dynamics of thin sheets of fluid iii. disintegration of fluid sheets. *Proc. Roy. Soc. London A* **253**, 253–313.
- UKIWE, C. & KWOK, D. Y. 2004 On the maximum spreading diameter of impacting droplets on well-prepared solid surfaces. *Langmuir* **21**, 666–673.
- WORTHINGTON, A. 1876 On the form assumed by drops of liquids falling vertically on a horizontal plate. *Proc. R. Soc. Lond.* **25**, 261–271.